JOURNAL OF SOLID STATE CHEMISTRY **105**, 78–91 (1993)

Crystal Structures and Magnetic Properties of CrO_4^{4-}-Containing Oxides: Sr_2CrO_4, Ba_2CrO_4, and Ba_3CrO_5

GUO LIU, J. E. GREEDAN, AND WENHE GONG

Institute for Materials Research, McMaster University, 1280 Main Street West, Hamilton, Ontario L8S 4M1, Canada

Received August 21, 1992; in revised form October 26, 1992; accepted October 28, 1992

Refinement of the crystal structures of Ba_2CrO_4 and Ba_3CrO_5 using powder neutron diffraction data has confirmed that the former is isostructural with β-K_2SO_4 and the latter isostructural with Cs_3CoCl_5. Ba_2CrO_4 is orthorhombic, *Pnma* (No. 62), $Z = 4$ with $a = 7.6285(5)$ Å, $b = 5.9136(5)$, $c = 10.4639(8)$, and $V = 472.04(5)$ Å^3; Ba_3CrO_5 is tetragonal, *I4/mcm* (No. 140), $Z = 4$ with $a = 7.3033(3)$ Å, $c = 11.6704(6)$, $V = 622.48(4)$ Å^3 from powder Guinier X-ray diffraction data. Magnetic properties of Sr_2CrO_4, Ba_2CrO_4, and Ba_3CrO_5 were examined down to 2–5 K. The structures and magnetic properties of Sr_2CrO_4 and Ba_2CrO_4 are compared with their vanadium analogues β-Sr_2VO_4 and β-Ba_2VO_4. Unlike isostructural β-Sr_2VO_4 which contains the $V_2O_8^{8-}$ dimer, Sr_2CrO_4 contains truly isolated CrO_4^{4-} tetrahedra and its magnetic behavior can be best described as a dimerized chain. Ba_2CrO_4 and Ba_3CrO_5 also contain isolated CrO_4^{4-} tetrahedra. Ba_2CrO_4 is paramagnetic down to 5 K. Ba_3CrO_5 undergoes long-range magnetic order at ~8 K, a temperature range significantly higher than that of isostructural Rb_3CoCl_5 and Cs_3CoX_5(X = Cl, Br). © 1993 Academic Press, Inc.

Introduction

We recently reported the synthesis and characterization of the Sr_2CrO_4-type Sr_2VO_4(β-Sr_2VO_4) (*1*) and the Ca_2SiO_4-type Ba_2VO_4 (β-Ba_2VO_4) (*2*). The β-Sr_2VO_4 structure is related to β-K_2SO_4, and an interesting $V_2O_8^{8-}$ dimer (Scheme I) is found (*2*). The true symmetry of β-Ba_2VO_4, which was previously thought to be isostructural with the orthorhombic β-K_2SO_4, is actually monoclinic, isostructural with β-Ca_2SiO_4 and its magnetic behavior can be best approximated as a Heisenberg infinite linear chain (*2*). These findings raised questions and interest about the Cr(IV) analogues. For example, although Ba_2CrO_4 had long been thought to be isostructural with β-K_2SO_4, there was no detailed structural information, and not even a powder pattern in the JCPDS files. The structure of Sr_2CrO_4 was solved previously using single crystal X-ray diffraction data. The magnetic properties of these Cr(IV) oxides were unknown. Thus we carried out a comparative study of the Cr(IV) analogues of the V(IV) oxides, Sr_2CrO_4 and Ba_2CrO_4. We were also interested in the magnetic properties of Ba_3MO_5 (M = V, Cr), which have, presumably, the Cs_3CoCl_5 structure, because the cobalt halides A_3CoX_5 (A = Rb, Cs; X = Cl, Br) are well-known two- and three-dimensional Ising systems (*3–5*). One common feature of these chromium and vanadium oxides is the existence of isolated MO_4^{4-} tetrahedra. In this paper we report the synthesis of phase-pure specimens of the title compounds and present the results of the structure refinement using powder neutron diffraction data and of studies of their magnetic properties.

0022-4596/93 $5.00

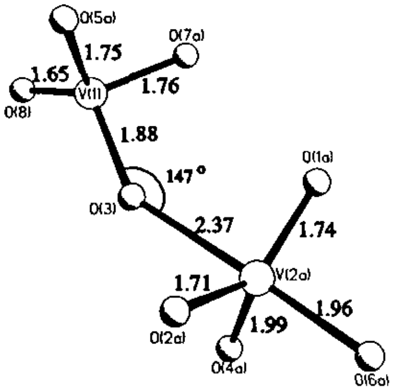

SCHEME I. $V_2O_8^{8-}$ dimer in β-Sr_2VO_4 (bond lengths in Å).

Experimental

Synthesis

Sr_2CrO_4. Six to seven grams of polycrystalline Sr_2CrO_4 were synthesized according to Wilhelmi (*6*). A stoichiometric mixture of $SrCrO_4$ (prepared by heating a $2SrCO_3$ + Cr_2O_3 mixture in O_2 at 800°C for 20 hr), Cr_2O_3 (Fisher Certified), and $5Sr(OH)_2 \cdot 8H_2O$ (Johnson Matthey Electronics) was ground intimately, pelleted, and heated in a platinum crucible in N_2 at 1000°C overnight and then cooled slowly.

Ba_2CrO_4. This phase was synthesized by two different methods. The first was based on that of Scholder and Sperka (*7*). Ten to fifteen grams of a stoichiometric mixture of $BaCrO_4$, Cr_2O_3, and $5Ba(OH)_2 \cdot 8H_2O$ (Fisher Scientific, 99.3%) were ground intimately, pelleted, and evacuated overnight to dehydrate $Ba(OH)_2 \cdot 8H_2O$, partially. The resulting powder was pelleted again, confined in a Pt crucible, which was secured in an alumina boat, heated in N_2 at 950°C overnight, and cooled slowly. In the second method 8–9 g of a 4 : 1 molar mixture of $BaCO_3$ (AESAR, Johnson Matthey Inc., 99.9%) and Cr_2O_3 were heated slowly (within 4 hr) in hydrogen to 900°C for 24 hr, and then 10% more Cr_2O_3 was added to the pulverized product, and the mixture fired in N_2 for 24 hr.

Ba_3CrO_5. The compound was synthesized by reducing pellets of either a 1 : 1 molar mixture of Ba_2CrO_4 and $BaCO_3$ or a 6 : 1 mixture of $BaCO_3$ and Cr_2O_3 with H_2 at 1000°C for 20 hr.

X-Ray and Neutron Diffraction

All specimens were examined routinely using a Guinier–Hägg camera (IRDAB XDC700) with Cu$K\alpha$1 radiation and a Si standard. The Guinier data were read with a computer-controlled automated LS-20 type line scanner (KEJ Instruments, Täby, Sweden). Neutron diffraction data for powder specimens were collected at the McMaster Nuclear Reactor. The refinement was effected on a VAX computer using LHPM1 of Hill and Howard (*8*) which is a modified version of DBW3.2 due to Wiles and Young (*9*). Details of the neutron data collection and refinement methods have been described previously (*10*). Neutron scattering lengths (fm) used were 5.25, 3.635, and 5.805 for Ba, Cr, and O, respectively (*11*).

Magnetic Susceptibility Measurement

Susceptibility data were obtained using a Quantum Design SQUID magnetometer in the temperature range 2–5 to 300 K using pelleted specimens at an applied magnetic field of 0.2 T. Diamagnetic corrections were applied.

Results and Discussion

Guinier X-ray diffraction data suggested that all the Cr(IV) oxide specimens were single phases. The powder pattern of Sr_2CrO_4 matched that reported previously (*12*). Since a large amount of moisture was released during the reaction involving $Ba(OH)_2 \cdot 8H_2O$, it is important to heat the mixture slowly. The H_2 reduction product of a stoichiometric mixture of $4BaCO_3$ and Cr_2O_3 contained trace amounts of Ba_3CrO_5. When 10% excess Cr_2O_3 was used in the second stage heating in N_2, phase-pure Ba_2CrO_4 was obtained. The synthesis of

Ba_2CrO_4 and Ba_3CrO_5 using $BaCO_3$ and Cr_2O_3 probably involves the initial oxidation of Cr_2O_3 by $BaCO_3$ and the subsequent reduction of the oxidized chromate by H_2. It is worth noting that the method described by Scholder and Sperka (*7*) for the synthesis of Ba_3CrO_5, heating in N_2 a stoichiometric mixture of either $BaCrO_4$, Cr_2O_3, and $8Ba(OH)_2$ or even Ba_2CrO_4 and $Ba(OH)_2$, produced very impure specimens in which Ba_3CrO_5 was observed only as a minor phase. Attempts to synthesize phase-pure Ba_3VO_5 under various conditions were unsuccessful. Ba_3VO_5 was only obtained as a mixture with Ba_2VO_4 and other unidentified impurities when a $3BaCO_3$ and $Ba_3V_2O_8$ mixture was reduced by H_2 at 1200°C in a Mo tube. This problem had been noted by Jansen and co-workers (*13*), who reported the synthesis of Ba_3VO_{4+x} by a BaO and VO reaction *in vacuo*.

Crystal Structures

For Ba_2CrO_4 33 reflections were indexed completely by TREOR (*14*) based on an orthorhombic symmetry with a = 10.466(2) Å, b = 7.627(1), and c = 5.915(1) and reasonably high figures of merit, $M(33)$ = 18 and $F(33)$ = 22. The cell parameters suggested the similarity of the structure with α-Ba_2TiO_4 which is isostructural with β-K_2SO_4 (*15*). Observed intensities well matched those simulated using the LAZY-PULVERIX programs (*16*) and the β-K_2SO_4 structure model (*17*). Final refinement results using powder neutron diffraction data confirmed the structure.

Twenty reflections of Ba_3CrO_5 were also indexed completely by TREOR based on a tetragonal unit cell with a = 7.3039(2) Å, c = 11.6704(5), and figures of merit $M(20)$ = 67 and $F(20)$ = 61. The Cs_3CoCl_5-type structure (18) for Ba_3CrO_5 has been confirmed from the powder neutron data refinement as well. The similarity of the powder pattern of Ba_3VO_5 with that of Ba_3CrO_5 was obvious. Refined tetragonal lattice parameters for Ba_3VO_5 are a = 7.2987(5) Å and c = 11.8306(9). Data collection conditions and refinement details, including least-squares refined lattice parameters using Guinier powder data for Ba_2CrO_4 and Ba_3CrO_5, are summarized in Table I.

TABLE I

DATA COLLECTION CONDITIONS AND REFINEMENT DETAILS FOR Ba_2CrO_4 AND Ba_3CrO_5

Parameters	Ba_2CrO_4		Ba_3CrO_5	
Space group	*Pnma* (No. 62)		*I4/mcm* (No. 140)	
Diffraction	Neutron	X-ray (Guinier)	Neutron	X-ray (Guinier)
λ (Å)	1.3913	1.5406	1.3950	1.5406
Cell parameters				
a (Å)	7.626(2)	7.6285(5)	7.308(1)	7.3033(3)
b (Å)	5.913(2)	5.9136(5)		
c (Å)	10.457(3)	10.4639(8)	11.669(2)	11.6704(6)
V (Å^3)	471.5(2)	472.04(5)	623.1(2)	622.48(4)
2θ range (°)	10–91		10–113	
Step size (°)	0.10		0.10	
Nuclear R_N	0.0212		0.0277	
Weighted profile R_{WP}	0.0399		0.0594	
Profile R_P	0.0317		0.0478	
Expected R_E	0.0229		0.0310	
No. of profile points N	811		1031	
No. of parameters refined	31		202	
Independent reflections	296		169	

Note. $R_N = R_B = \Sigma |I_{obs} - I_{cal}|/\Sigma I_{obs}$. $R_{WP} = \{[\Sigma w(Y_{obs} - Y_{cal}/c)^2]/\Sigma wY_{obs}^2\}^{1/2}$. $R_P = \Sigma |Y_{obs} - Y_{cal}/c|/\Sigma Y_{obs}$. $R_E = [(N - P)/\Sigma wY_{obs}^2]^{1/2}$.

TABLE II

ATOMIC PARAMETERS FOR Ba_2CrO_4 AND Ba_3CrO_5 FROM NEUTRON POWDER DIFFRACTION DATA

Compound	Atom	Site	*x*	*y*	*z*	*B* (Å²)
Ba_2CrO_4	Ba(1)	4(*c*)	0.147(1)	0.25	0.080(2)	2.7(4)
	Ba(2)	4(*c*)	−0.011(2)	0.25	0.6942(9)	1.1(2)
	Cr	4(*c*)	0.220(2)	0.25	0.431(2)	2.0(3)
	O(1)	4(*c*)	−0.008(1)	0.25	0.416(1)	2.7(2)
	O(2)	4(*c*)	0.314(2)	0.25	0.576(1)	0.4(2)
	O(3)	8(*d*)	0.308(1)	0.006(2)	0.3500(6)	1.5(1)
Ba_3CrO_5	Ba(1)	4(*a*)	0	0	0.25	1.4(1)
	Ba(2)	8(*h*)	0.3211(4)	0.8211(4)	0	0.56(9)
	Cr	4(*b*)	0	0.5	0.25	1.5(2)
	O(1)	4(*c*)	0	0	0	1.7(1)
	O(2)	16(*l*)	0.1357(3)	0.6357(3)	0.1576(3)	1.65(6)

Atomic parameters for Ba_2CrO_4 and Ba_3CrO_5 are listed in Table II. Selected bond distances and bond angles are listed in Table III. Neutron diffraction patterns for Ba_2CrO_4 and Ba_3CrO_5 are plotted in Figs. 1 and 2, respectively.

Ba_2CrO_4. To compare with the β-Ba_2VO_4 structure (*2*), the Ba_2CrO_4 structure is viewed down the less convenient *a*-axis as shown in Fig. 3. Apparently, the two structures are very similar. Like β-Ba_2VO_4, there exist two types of Ba–O coordination in Ba_2CrO_4, $Ba(1)O_{10}$ and $Ba(2)O_9$, both of which are loosely bonded. Ba(2) is relatively more tightly bonded to oxygen as indicated by the shorter average Ba(2)–O bond length and its lower isotropic temperature factor compared with corresponding values for Ba(1). This is characteristic of the β-K_2SO_4-related structures such as β-Ba_2VO_4 (*2*) and β-Sr_2SiO_4 (*19*). The average Ba(1)–O and Ba(2)–O bond distances of Ba_2CrO_4 are

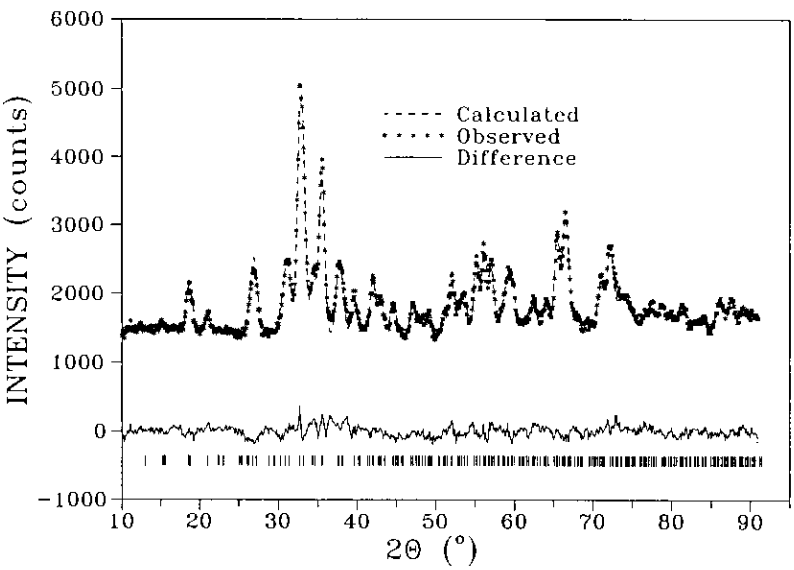

FIG. 1. The neutron powder pattern for Ba_2CrO_4 with Bragg positions marked with parallel bars below the difference pattern.

TABLE III

SELECTED BOND DISTANCES AND BOND ANGLES FOR Ba_2CrO_4 AND Ba_3CrO_5

Ba_2CrO_4		Ba_3CrO_5	
Ba(1)–O(1)*f*	2.631(16)	Ba(1)–O(1)	2.9172(4)
Ba(1)–O(2)*c*	2.972(2)	Ba(1)–O(1)*f*	2.9172(4)
Ba(1)–O(2)*d*	2.972(2)	Ba(1)–O(2)*c*	3.039(3)
Ba(1)–O(2)*f*	3.019(20)	Ba(1)–O(2)*b*	3.039(1)
Ba(1)–O(3)	3.401(18)	Ba(1)–O(2)*d*	3.039(1)
Ba(1)–O(3)*c*	2.860(18)	Ba(1)–O(2)*g*	3.039(2)
Ba(1)–O(3)*f*	3.053(14)	Ba(1)–O(2)*h*	3.039(3)
Ba(1)–O(3)*i*	3.401(18)	Ba(1)–O(2)*i*	3.039(1)
Ba(1)–O(3)*i*	2.860(18)	Ba(1)–O(2)*j*	3.039(1)
Ba(1)–O(3)*k*	3.053(14)	Ba(1)–O(2)*k*	3.039(2)
Average	3.022(14)	Average	3.014(2)
Ba(2)–O(1)	2.914(17)	Ba(2)–O(1)*l*	2.686(1)
Ba(2)–O(1)*g*	3.174(6)	Ba(2)–O(1)*o*	2.686(1)
Ba(2)–O(1)*h*	3.174(6)	Ba(2)–O(2)	2.656(4)
Ba(2)–O(2)	2.767(19)	Ba(2)–O(2)*m*	2.961(4)
Ba(2)–O(2)*l*	2.750(17)	Ba(2)–O(2)*n*	2.961(3)
Ba(2)–O(3)*h*	2.763(14)	Ba(2)–O(2)*p*	2.656(4)
Ba(2)–O(3)*b*	2.712(12)	Ba(2)–O(2)*q*	2.961(3)
Ba(2)–O(3)*m*	2.763(14)	Ba(2)–O(2)*r*	2.961(4)
Ba(2)–O(3)*n*	2.712(12)		
Average	2.859(13)	Average	2.816(2)
Cr–O(1)	1.745(19)	Cr–O(2)	1.769(2)
Cr–O(2)	1.674(24)	Cr–O(2)*e*	1.769(4)
Cr–O(3)	1.801(14)	Cr–O(2)*h*	1.769(2)
Cr–O(3)*i*	1.801(14)	Cr–O(2)*s*	1.769(4)
Average	1.755(18)	Average	1.769(3)
O(1)–Cr–O(2)	120.7(13)	O(2)–Cr–O(2)*e*	111.8
O(1)–Cr–O(3)	109.0(8)	O(2)–Cr–O(2)*h*	104.9(2)
O(1)–Cr–O(3)*i*	109.0(8)	O(2)–Cr–O(2)*s*	111.8(1)
O(2)–Cr–O(3)	105.5(8)	O(2)e–Cr–O(2)*h*	111.8(1)
O(2)–Cr–O(3)*i*	105.5(8)	O(2)e-Cr-O(2)*s*	104.9(1)
O(3)–Cr–O(3)*i*	106.2(10)	O(2)h-Cr-O(2)*s*	111.8
Average	109.3(8)	Average	109.5(1)

close to those in β-Ba_2VO_4. The CrO_4^{4-} polyhedra in Ba_2CrO_4 are isolated as the VO_4^{4-} in β-Ba_2VO_4 (*2*) and TiO_4^{4-} in Ba_2TiO_4 (*20*). The average Cr–O bond distance of 1.76(2) Å is slightly shorter than that of $Cr(1)O_4^{4-}$ in Sr_2CrO_4 (1.80 Å) and significantly shorter than the $Cr(2)O_4^{4-}$ in Sr_2CrO_4 (1.85 Å), but is comparable with the V–O distance in β-Ba_2VO_4 (1.76(3) Å) and the $V(1)O_4^{4-}$ in Sr_2VO_4 (1.76(2) Å). The CrO_4^{4-} tetrahedron is rather irregular with O–Cr–O bond angles ranging from 105.5 to 120.7°. Even though severe angular distortion was also observed for VO_4^{4-} in β-Ba_2VO_4, there exists a significant difference in the *M*–O bond lengths between the CrO_4^{4-} and the VO_4^{4-} polyhedra. The CrO_4^{4-} tetrahedra in Ba_2CrO_4 include one short Cr–O bond (1.67 Å) while β-Ba_2VO_4 has one long V–O bond (1.84(3) Å). One short bond (*M*(1)–O(8)) was also observed for the MO_4^{4-} tetrahedra in Sr_2CrO_4 (1.66–1.67 Å) (*6*) and β-Sr_2VO_4 (1.65(3) Å) (*1*). These results suggest that even though Cr(IV) and V(IV) have very

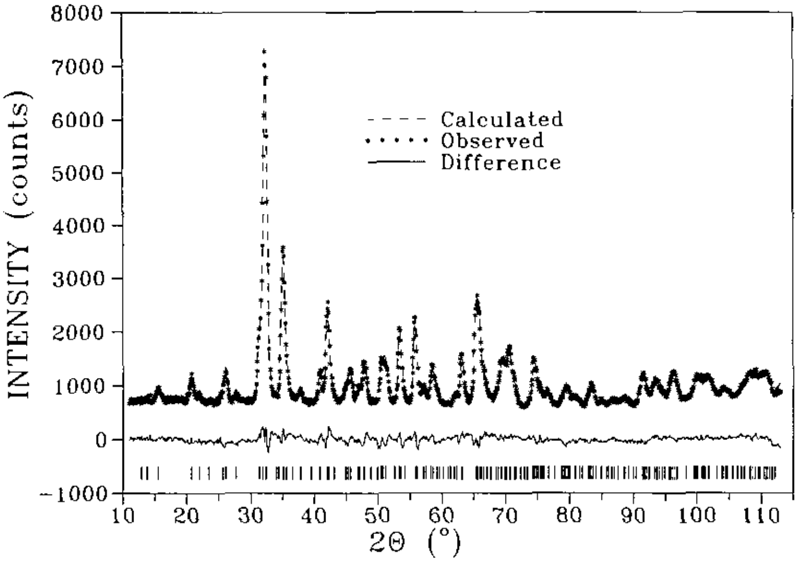

FIG. 2. The neutron powder pattern for Ba_2CrO_5 with Bragg positions marked with parallel bars below the difference pattern.

similar ionic radii (the value for 4-coordinated V(IV) is not available, but $r(V^{4+}_{CN=6}) = 0.72$ Å and $r(Cr^{4+}_{CN=6}) = 0.69$ Å) (*21*), and Ba_2CrO_4 and β-Ba_2VO_4 have similar structures, the coordination environment of the transition metal is sensitive to the small difference in the size of *M*(IV), and probably to the electronic structure as well. The difference in symmetry and the MO_4^{4-} coordination polyhedra between Ba_2CrO_4 and β-Ba_2VO_4 results in a further separation of the CrO_4^{4-} tetrahedra in the actually smaller-sized unit cell of Ba_2CrO_4 as compared to the β-Ba_2VO_4. This is evidenced by the fact that the shortest contact distance between oxygens of neighboring CrO_4^{4-} tetrahedra (O(3) · · · O(2), 3.35–3.37(4) Å) is longer than that between the VO_4^{4-} polyhedra in β-Ba_2VO_4 (O(3) · · · O(4*h*), 3.16(3) Å. Fig. 3). This result is expected to weaken the magnetic exchange interaction between the tetrahedra in Ba_2CrO_4.

Sr_2CrO_4. This structure can be described as a strongly distorted superstructure of β-K_2SO_4, and is thus related to Ba_2CrO_4. Details of the Sr_2CrO_4 structure and its relationship with β-K_2SO_4 have been described previously (*6*). Some crystallographic data of the A_2BO_4-type compounds (*A* = Sr, Ba; *B* = V, Cr) are compared in Table IV.

It is worth examining the CrO_4^{4-} polyhedra in Sr_2CrO_4 to facilitate the discussion and comparison of its magnetic properties with those of β-Sr_2VO_4. The structure is shown in Fig. 4. The two types of distorted

TABLE IV

CRYSTALLOGRAPHIC DATA OF THE A_2BO_4 COMPOUNDS (*A* = Sr, Ba; *B* = V, Cr)

Compound	Space group	*a* (Å)	*b* (Å)	*c* (Å)	β(°)	Reference
β-Sr_2VO_4	*Pna*2$_1$	14.092(4)	5.806(2)	10.106(3)		(*1*)
Sr_2CrO_4	*Pna*2$_1$	14.182(10)	5.788(30)	10.100(20)		(*6*)
β-Ba_2VO4	P2$_1$/*n*	6.0191(7)	7.6494(7)	10.465(1)	92.39(1)	(*2*)
Ba_2CrO_4	*Pmnb*	5.9136(5)	7.6285(5)	10.4639(8)		This work

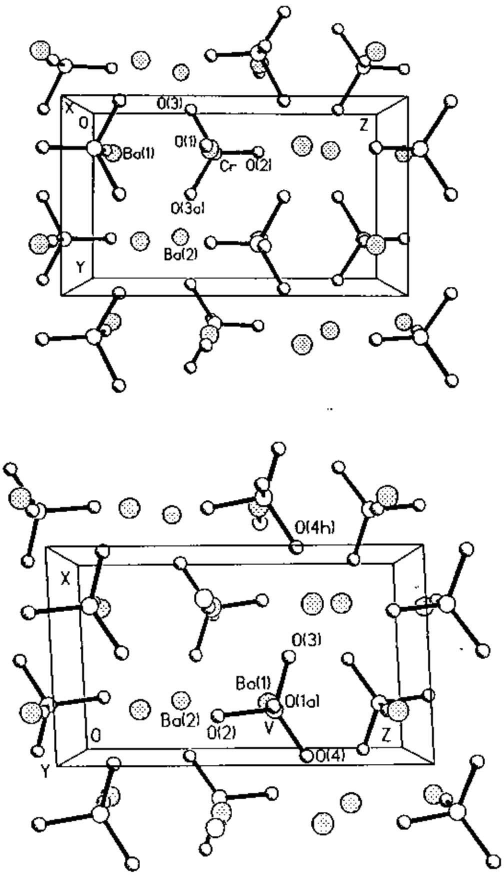

FIG. 3. The Ba_2CrO_4 (top) and the β-Ba_2VO_4 (bottom, β = 92.39(1)°) structures as viewed along the a- and b-axes, respectively.

CrO_4^{4-} tetrahedra, as already mentioned above, have apparently different average bond lengths. Similar to the $V(2)O_4^{4-}$ in β-Sr_2VO_4, the $Cr(2)O_4^{4-}$ distorts the most. The Cr(2)–O bond lengths range from 1.67 to 1.95 Å, and O–Cr(2)–O angles range from 97 to 126° as compared to the 109.8° for a regular tetrahedron. However, the M(2)–O(3) bridge that is responsible for the formation of the $V_2O_8^{8-}$ dimer in β-Sr_2VO_4 is significantly longer for M = Cr (2.74(3) Å) than for M = V (2.37(3) Å). It is fair to conclude that there is no $Cr_2O_8^{8-}$ dimer in Sr_2CrO_4 even though the bridging may still be responsible for the magnetic superexchange in Sr_2CrO_4.

Ba_3CrO_5. The Ba_3CrO_5 structure is also characterized by isolated CrO_4^{4-} tetrahedra. The $Ba(1)O_{10}$ and $Ba(2)O_8$ polyhedra are similar to those in Ba_2CrO_4. Again the Ba(2) is more tightly bonded with oxygen atoms and thus has a lower temperature factor than Ba(1). But the CrO_4^{4-} tetrahedra in Ba_3CrO_5 are far more regular than those in Ba_2CrO_4. The Cr–O bond lengths are uniform. A minor distortion exists only in the O–Cr–O angles, 104.9 and 111.8°, which are about the same as those for $CoCl_4^{2-}$ in Cs_3CoCl_5 (106.0 and 111.2°) (*18*). A unit cell is shown in Fig. 5 with the CrO_4^{4-} tetrahedra outlined. It can be described as a layered structure consisting of layers of nonmagnetic Ba^{2+} ions and magnetic CrO_4^{4-} groups separated by nonmagnetic layers of Ba^{2+} and O^{2-} ions. The shortest Cr–Cr distance is $a' = \sqrt{2} \cdot a/2 = 5.1642$ Å within a magnetic layer, and $c' = c/2 = 5.8352$ Å between two adjacent magnetic layers. Each CrO_4^{4-} group has six CrO_4^{4-} nearest neighbors (nn). Due to the closeness of the two distances and the arrangement of the Cr ions, the magnetic sublattice is usually treated as a simple cube (sc). Such a sublattice is outlined in Fig. 5 with dotted lines. The c'/a' ratio is 1.130 for Ba_3CrO_5, 1.146 for Ba_3VO_5, 1.116 for Cs_3CoCl_5, and 1.115 for Cs_3CoBr_3. It can

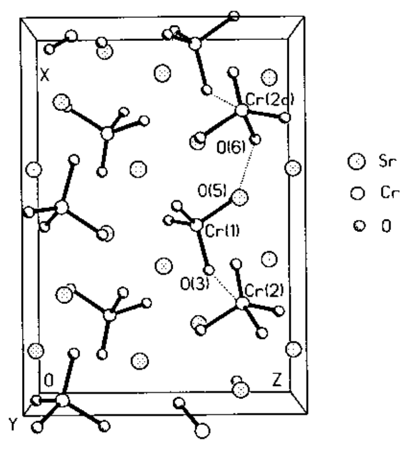

FIG. 4. The Sr_2CrO_4 structure as viewed along the b-axis. The dotted lines indicate a possible dimerized chain.

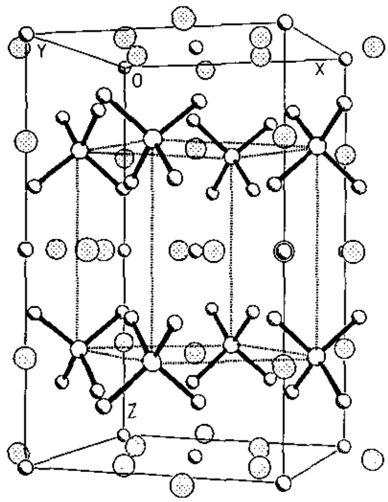

FIG. 5. A perspective view of the Ba_3CrO_5 structure. A magnetic subcell is outlined with the dotted lines.

be seen from these values that even though the oxides deviate from a simple cube more than the cobalt halides, the arrangement of magnetic ions in the oxides is still predominantly three dimensional. The superexchange pathways within and between the layers of MO_4^{4-} ions are not equivalent; however, both two-dimensional and three-dimensional pathways have been found in the halides as discussed in the following sections.

Magnetic Properties

Sr_2CrO_4. The temperature dependence of the magnetic susceptibility of Sr_2CrO_4 is shown in Fig. 6. There exists a broad maximum at ~13 K. Neutron scattering experiments at 9 K revealed the absence of long-range magnetic order. Therefore, the observed maximum is indicative of short-range order. This susceptibility maximum temperature is significantly lower than that for β-Sr_2VO_4 (~60 K) (*1*). Furthermore, the susceptibility curve cannot be fitted satisfactorily to a simple Heisenberg dimer model like that of β-Sr_2VO_4. Attempts to fit the susceptibility data to either a Heisenberg infinite linear chain (1D) or a Heisenberg square plane (2D) also failed. The failure of the dimer model is consistent with the crystal structure of Sr_2CrO_4 as pointed out previously. But the susceptibility data can be fitted reasonably well to a modified dimer model-*a* dimerized chain also shown in Fig. 6. In this model it is assumed that the magnetic interactions are pseudo-one-dimensional, but due to alternating short

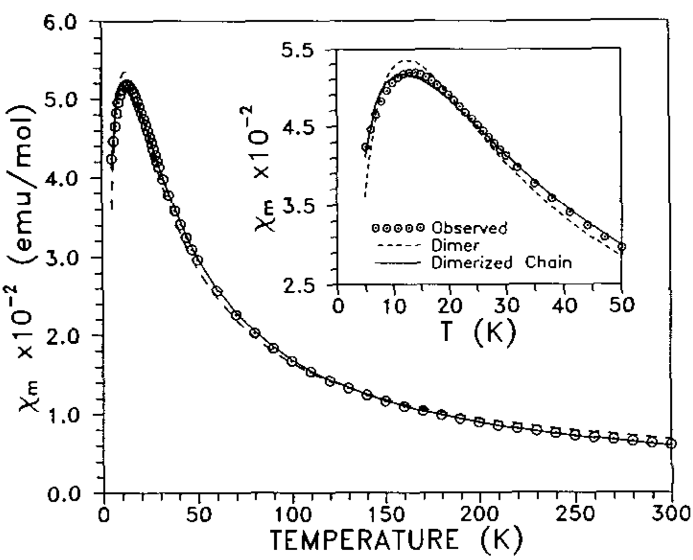

FIG. 6. Temperature dependence of the magnetic susceptibility of Sr_2CrO_4.

(Cr(2)–O(3)–Cr(1)) and long (Cr(1)–O(5) · · · O(6)–Cr(2)) distances, the interactions retain a certain "dimer" characteristic. Such a mechanism is depicted in Fig. 4 as dotted lines. According to Vasilevesky *et al.* (*22*) the analytical form for a dimerized chain is

$$\chi_m = \frac{\chi_m(\text{dimer})T}{T - 2ZJ'/3k},$$

where J' is the inter-dimer exchange parameter, Z the number of nearest neighbors (2 for a dimerized chain), and χ_m(dimer) the susceptibility for 2 mol of Sr_2CrO_4, which has the expression according to O'Connor (*23*)

$$\chi_m(\text{dimer}) = A\frac{2e^{2x} + 10e^{6x}}{1 + 3e^{2x} + 5e^{6x}}$$

$$A = \frac{N\bar{g}^2\mu_B^2}{kT}, \quad x = \frac{J}{kT},$$

where J is the intra-dimer exchange parameter, $\bar{g}$ the powder-averaged g-factor, and other symbols have their usual meanings. This relationship holds for $|J| \gg |J'|$. The fit gave $\bar{g} = 1.93$, $J/k = -9.07$ K, and $J'/k = 2.49$ K. The condition $|J| \gg |J'|$ is not quite well satisfied. However, this model is the best approximation we can have thus far. The agreement factor for the fitting, defined as

$$R(\%) = 100\sqrt{\sum(\chi_{obs} - \chi_{cal})^2 \Big/ \sum \chi_{obs}^2},$$

is 1.29 for the dimerized chain as compared to $R(\%) = 3.53$ for the best fit using the simple dimer model. The fitting results indicate that although the antiferromagnetic intra-dimer exchange still predominates, there is a weak inter-dimer ferromagnetic interaction which probably suggests that the "dimers" are closer than those in β-Sr_2VO_4. This can probably be understood by the lengthening of the "dimer" bridge. Relevant bond distances and bond angles are shown below.

(°) 127.9 100.2 89.1 103.4
(Å) 2.74 1.83 1.86 2.95 1.95
Cr(2)—O(3)—Cr(1)—O(5) · · · O(6)—Cr(2)—O(3)—Cr(1)—O(5) · · ·
↑ ↓ ↓ ↑

The temperature dependence of the inverse susceptibility of Sr_2CrO_4 is rather peculiar (Fig. 7). Above the susceptibility maximum temperature no linear region can be seen clearly. The curve can be fitted to the Curie–Weiss law if a temperature-independent term is included. The fit gave $C = 0.976(2)$ cm^3 · K/mole, $\theta = -16(1)$ K, $\chi_{TIP} = 7.3(5) \times 10^{-4}$ cm^3/mole. The magnetic moment estimated from the Curie–Weiss constant C is thus $\mu_{eff} = 2.79$ μ_B, which is in good agreement with the theoretical spin-only moment of 2.83 μ_B for a d^2 ion. The field dependence of the magnetic moment of Sr_2CrO_4 is shown in Fig. 8. No spin–flop transition is observed since the curve is nearly a straight line, which suggests that no long-range antiferromagnetic order exists at 5 K, consistent with the low-temperature neutron experiment result.

Ba_2CrO_4. The temperature dependence of the inverse susceptibility is plotted in Fig. 9. The data show a distinct curvature similar to that of Sr_2CrO_4, but less pronounced. The 40–300 K data were fitted to the Curie–Weiss law with a temperature-independent term included. This gave $C = 0.818(4)$ cm^3 · K/mole, $\theta = -9.2(3)$ K, and $\chi_{TIP} = 2.85(2) \times 10^{-4}$ cm^3/mole. The estimated effective magnetic moment is 2.56 μ_B, slightly lower than the spin-only value for Cr(IV). It is worth noting that even though the Curie–Weiss law fits suggest antiferromagnetic interactions, no suscepti-

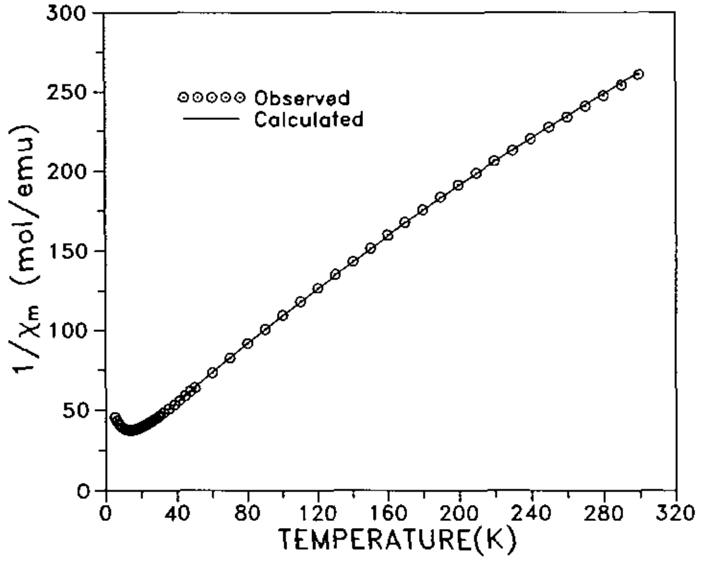

FIG. 7. Temperature dependence of the inverse susceptibility of Sr_2CrO_4.

bility maximum was observed for Ba_2CrO_4 down to 5 K. This is in contrast to β-Ba_2VO_4 which displays a susceptibility maximum at ~11 K and pseudo-one-dimensional short-range order (*2*), and may be due to the increased distances between MO_4^{4-} tetrahedra in the chromium compound relative to the vanadium compound as mentioned earlier.

Ba_3CrO_5. Magnetic susceptibility data of the low-temperature range for Ba_3CrO_5 are plotted in Fig. 10. There exists a relatively sharp maximum near 8 K. An attempt to fit the susceptibility data to a Heisenberg square planar lattice similar to that in Cs_3CoBr_5 was unsuccessful. Instead it most likely signals the onset of a long-range mag-

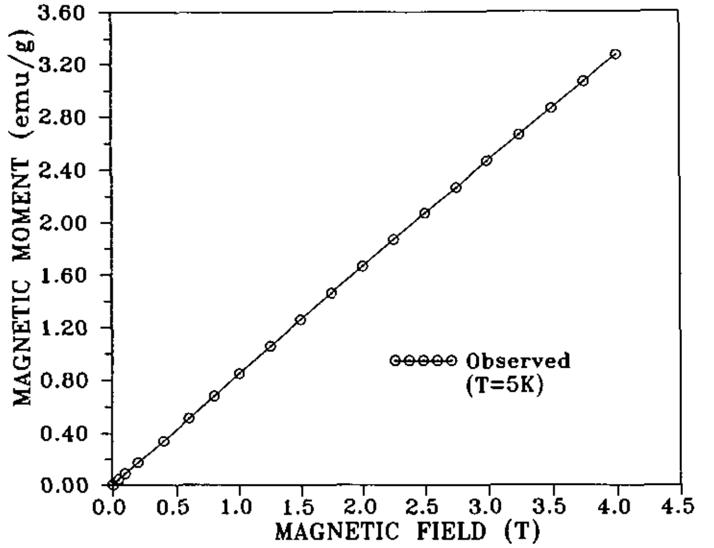

FIG. 8. Field dependence of the magnetic moment of Sr_2CrO_4 at 5 K showing the absence of a spin–flop transition.

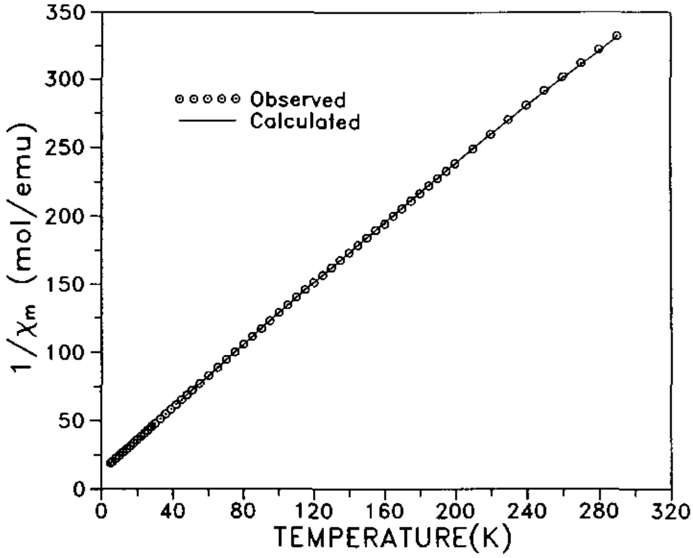

FIG. 9. Temperature dependence of the inverse susceptibility of Ba_2CrO_4.

netic order similar to that observed in Cs_3CoCl_5 (*4*, *5*). This effect can be seen clearly in a plot of $d(\chi \cdot T)/dT$ vs T as shown in Fig. 10, which according to Fisher (*24*) has the same functional form as the magnetic heat capacity near the critical temperature T_c. The lambda (λ) shape anomaly at *$T_c \approx$ 8K is obvious and indicates a phase* transition.

The inverse susceptibility data of Ba_3CrO_5 are plotted against temperature in Fig. 11. There appears to be a change in slope at ~120 K. The high-temperature (140–300 K) data were fitted to the Curie–Weiss law. The

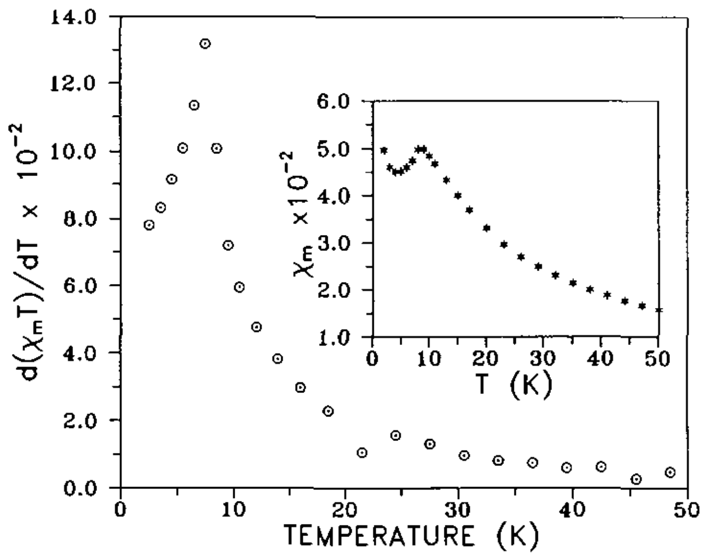

FIG. 10. Fisher's heat capacity obtained for Ba_3CrO_5 showing a λ anomaly at ~8 K. The corresponding sharp susceptibility maximum is shown in the insert.

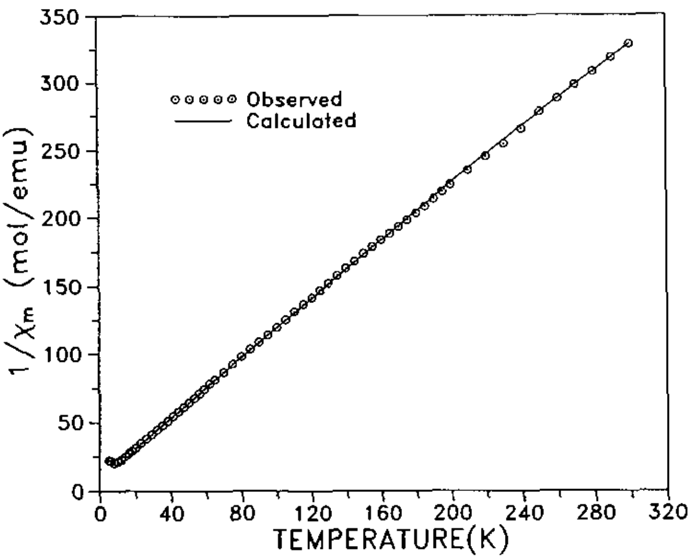

FIG. 11. Temperature dependence of the inverse susceptibility of Ba_3CrO_5. The calculated curve includes a TIP contribution.

fittings gave $C = 0.973(6)$ $cm^3 \cdot K/mole$ ($\mu_{eff} = 2.79\ \mu_B$) and $\theta = -18.4(2)$ K. When a temperature-independent term is included, the data between 20–300 K can be fitted to the Curie–Weiss law with $C = 0.883(5)$ $cm^3 \cdot K/mole$ ($\mu_{eff} = 2.66\ \mu_B$), $\theta = -7.4(2)$ K, and $\chi_{TIP} = 1.70(2) \times 10^{-4}$ $cm^3/mole$. The calculated curve shown in Fig. 11 includes the TIP contribution. In view of the observation of TIP terms of similar magnitude in Sr_2CrO_4 and Ba_2CrO_4 this interpretation of the susceptibility curve seems more reasonable at present.

The isostructural Cs_3CoCl_5 and Rb_3CoCl_5

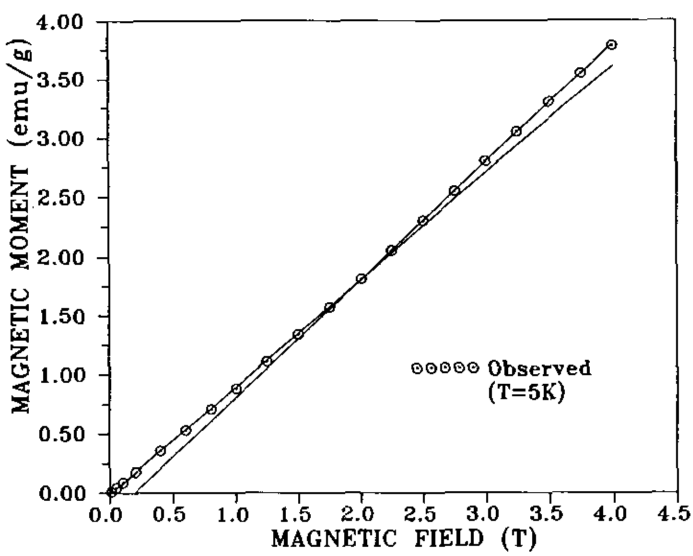

FIG. 12. Field dependence of the magnetic moment of Ba_3CrO_5 showing the spin–flop transition at $H \approx 2.25$ T.

are 3D Ising systems, while Cs_3CoBr_5 is a 2D Ising system (*3, 5*). Our magnetic data suggest that Ba_3CrO_5 is not likely an Ising system because a spin–flop transition has been observed, which is usually absent in an Ising system such as Cs_3CoBr_5 (*5*). The spin–flop transition is suggested by the change in slope at ~2.25 T in the field dependence of the magnetic moment of Ba_3CrO_5 (Fig. 12). Also the shape of the Fisher heat capacity, Fig. 10, indicates the absence of short-range correlations above the lambda anomaly. This suggests strongly that Ba_3CrO_5 is a 3D system like Cs_3CoCl_5. The proposed magnetic structure for the 3D Cs_3CoCl_3 is that there are four nearest neighbors coupled antiferromagnetically in the crystallographic *ab* plane and two nearest neighbors coupled ferromagnetically between the planes (5), but there are no neutron results to support this.

Ba_3VO_5. The unavailability of sufficiently pure Ba_3VO_5 specimens prevented obtaining reliable magnetic susceptibility data for Ba_3VO_5. A small hump at ~55 K was visible as shown in Fig. 13, which is probably an indication of a similar transition to that of Ba_3CrO_5. However, data from better quality specimens are necessary to give any meaningful interpretation of the origin of this local maximum.

In summary, the magnetic behavior of Sr_2CrO_4 is more complicated than the isostructural β-Sr_2VO_4, and its magnetic interactions are extended into longer ranges probably due to the elongation of the Cr(2)–O(3) bridge. Ba_3CrO_5 undergoes a long-range magnetic order at a rather high temperature compared to those of isostructural Cs_3CoX_5 (X = Cl, Br) and Rb_3CoCl_5 (all below 1.2 K). Thus Ba_3CrO_5 seems to be an appropriate candidate for the elucidation of the magnetic structure of the Cs_3CoCl_5-type compounds by low-temperature magnetic neutron scattering.

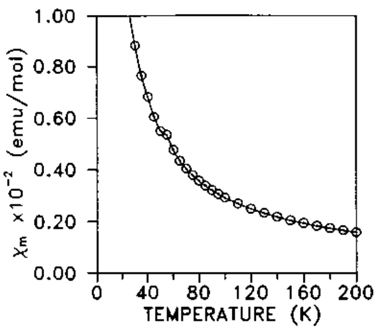

FIG. 13. Temperature dependence of the magnetic susceptibility of Ba_3VO_5 showing a hump at ~55 K.

Acknowledgments

The financial support of the Natural Science and Engineering Research Council of Canada and the Ontario Centre for Materials Research is acknowledged gratefully. We thank Professor C. V. Stager for use of the magnetometer.

References

1. WENHE GONG, J. E. GREEDAN, GUO LIU, AND M. BJORGVINSSON, *J. Solid State Chem.* **95,** 213 (1991).
2. GUO LIU AND J. E. GREEDAN, *J. Solid State Chem.* **103,** 228 (1993).
3. H. W. J. BLÖTE AND W. J. HUISKAMP, *Phys. Lett. A.* **29,** 304 (1969).
4. R. F. WIELINGA, H. W. J. BLÖTE, J. A. ROEST, AND W. J. HUISKAMP, *Physica* **34,** 223 (1967).
5. K. W. MESS, E. LAGENDIJK, D. A. CURTIS, AND W. J. HUISKAMP, *Physica* **34,** 126 (1967).
6. KARL-AXEL WILHELMI, *Ark. Kemi.* **26,** 157 (1966).
7. R. SCHOLDER AND G. SPERKA, *Z. Anorg. Allg. Chem.* **285,** 49 (1956).
8. R. J. HILL AND C. J. HOWARD, Australian Atomic Energy Commission Report No. M112, Lucos Heights Research Laboratories, New South Wales, Australia (1986).
9. D. B. WILES AND R. A. YOUNG, *J. Appl. Crystallogr.* **14,** 149 (1981).
10. J. N. REIMERS, J. E. GREEDAN, AND M. SATO, *J. Solid State Chem.* **72,** 390 (1988).
11. V. F. SEARS, *in* "Methods of Experimental Physics" (K. Skold and D. L. Price, Eds.), Vol. 23a, p. 521, Academic Press, San Diego (1986).
12. Powder Diffraction File Card 33-1324. JCPDS: International Centre for Diffraction Data, 1601 Park Lane, Swarthmore, PA 19081.
13. P. W. J. JANSEN, U. SPITSBERGEN, AND P. M. DE WOLFF, *Recl. Trav. Chim.* **84,** 821 (1965).
14. P. E. WERNER, L. ERIKSSON, AND M. WESTDAHL, *J. Appl. Crystallogr.* **18,** 367 (1985).
15. J. J. RITTER, R. S. ROTH, AND J. E. BLENDELL, *J. Am. Ceram. Soc.* **69,** 155 (1986); Powder Diffraction File Card 38-1481. JCPDS: International Cen-

tre for Diffraction Data, 1601 Park Lane, Swarthmore, PA 19081.
16. K. YVON, W. JEITSCHKO, AND E. PARTHÉ, *J. Appl. Crystallogr.* **10,** 73 (1977).
17. M. T. ROBINSON, *J. Phys. Chem.* **62,** 925 (1958).
18. B. N. FIGGIS, M. GERLOCH, AND R. MASON, *Acta Crystallogr.* **17,** 506 (1964).
19. M. CATTI, G. GAZZONI, AND G. IVALDI, *Acta Crystallogr. Sect. C* **39,** 29 (1983).
20. J. A. BLAND, *Acta Crystallogr.* **14,** 875 (1961).
21. R. D. SHANNON, *Acta Crystallogr. Sect. A* **32,** 751 (1976).
22. I. VASILEVESKY, N. R. ROSE, R. STENKAMP, AND R. D. WILLETT, *Inorg. Chem.* **30,** 4082 (1991).
23. C. J. O'CONNOR, *Prog. Inorg. Chem.* **29,** 203 (1982).
24. M. E. FISHER, *Philos. Mag.* **7,** 1731 (1962).